Contribution of Polarimetry and Multi-Incidence to Soil Moisture Estimation Over Agricultural Fields Based on Time Series of *L*-Band SAR Data

Hontao Shi, *Graduate Student Member, IEEE*, Juan M. Lopez-Sanchez, *Senior Member, IEEE*, Jie Yang, Pingxiang Li, Lingli Zhao, *Member, IEEE*, and Jinqi Zhao

***Abstract*—The alpha approximation method is known to be effective and simple for soil moisture retrieval from time series of synthetic aperture radar data. However, its accuracy is usually degraded by the scattering from vegetation, and it entails working with an underdetermined linear system when solving the unknown surface parameters. In this work, we study how the availability of fully polarimetric data and a diversity in incidence angles can help this method for soil moisture estimation. Results are obtained using data from the Soil Moisture Active Passive Validation Experiment 2012 campaign acquired by an air-borne *L*-band radar system. The assessment of the performance is based on *in situ* measurements over agricultural fields corresponding to five different crop types: bean, soybean, canola, corn, and wheat. The validation shows that, compared with the original method, the retrieval accuracy can be improved when the polarimetric decomposition is included in the approach. The combination of polarimetric decomposition and multi-incidence observations of enriched data provides the best performance, with a decrease in the final root-mean-square error between 0.4% and 5% with respect to single-pol and single-incidence data. Compared with HH, the results obtained for VV data present a higher accuracy for the overall crop types. The most noticeable improvement is achieved for corn, soybean and wheat, demonstrating the contribution of this extension of the original approach.**

***Index Terms*—Alpha approximation, multi-incidence, polarimetric decomposition (PD), soil moisture estimation, synthetic aperture radar (SAR), time series.**

Manuscript received August 28, 2020; revised October 13, 2020 and November 3, 2020; accepted November 4, 2020. Date of publication November 9, 2020; date of current version January 6, 2021. This work was supported in part by the Spanish Ministry of Science, Innovation and Universities, in part by the State Agency of Research (AEI), in part by the European Funds for Regional Development (EFRD) under Project TEC2017-85244-C2-1-P, in part by the National Natural Science Foundation of China under Grant 61971318, Grant 41771377, Grant 41901286, and Grant 42071295, and in part by the Key Laboratory of Surveying and Mapping Science and Geospatial Information Technology of Ministry of Natural Resources under Grant 201905 and Grant 201906. The work of Hongtao Shi was supported by the China Scholarship Council (CSC) for 14 months study at the University of Alicante, Spain. *(Corresponding author: Juan M. Lopez-Sanchez.)*

Hontao Shi, Jie Yang, Pingxiang Li, and Jinqi Zhao are with the State Key Laboratory of Information Engineering in Surveying, Mapping, and Remote Sensing, Wuhan University, Wuhan 430079, China (e-mail: sht9010@whu.edu.cn; yangj@whu.edu.cn; pxli@whu.edu.cn; masurq@whu.edu.cn).

Juan M. Lopez-Sanchez is with the Institute for Computing Research, University of Alicante, 03080 Alicante, Spain (e-mail: juanma-lopez@ieee.org).

Lingli Zhao is with the School of Remote Sensing and Information Engineering, Wuhan University, Wuhan 430079, China (e-mail: zhaolingli@whu.edu.cn).

Digital Object Identifier 10.1109/JSTARS.2020.3036732

I. Introduction

SURFACE soil moisture (SSM) is a critical variable in environmental and agricultural studies. Accurate knowledge of the spatial and temporal characteristics of SSM is crucial for many fields including meteorology, landslide monitoring, and drought prediction. Especially in agricultural applications, SSM is taken as an important feature for optimizing water usage efficiency [1]. Over the last four decades, considerable research efforts have been devoted to soil moisture estimation by means of synthetic aperture radar (SAR) and proved the potential of SAR data at *L*, *C*, and *X* bands for estimating SSM over bare and vegetated soils [2], [3]. The use of physical models (IEM, AIEM), semiempirical models (Oh, Dubois, and Shi) [4], decomposition theorems (Freeman–Durden, Yamaguchi, and Cloude–Pottier) [5]–[7], change detection techniques [8]–[10], and statistics-based methods [11]–[13] applied to multiple SAR observations have improved the capability to obtain SSM information at high spatial resolution (less than 10 m).

Generally, the SSM estimation from SAR for bare soils has been well proved, but estimation over moderate or dense vegetated areas is still a challenging task [14]. This is due to the influence of vegetation canopy structure, density, plant water content (PWC), biomass, etc. Particularly, the SSM estimation over agricultural areas is more complicated due to the continuous change of phenological stages of crops. For this case, a set of empirical scattering models, e.g., water could model (WCM), and model-based polarimetric decomposition (PD) techniques were proposed to decouple the effect of SSM on SAR backscatter from that of vegetation canopy. The empirical models obtained from the remote sensing measurements and *in situ* observations could be easily implemented to describe the nonlinear relationship between the backscattering coefficient and the surface parameters (e.g., soil roughness, vegetation, and soil moisture, etc.). However, an accurate estimation largely rely on the ancillary vegetation information (e.g., leaf area index and vegetation water content), and its robustness is usually limited because of the different conditions from field to field. Based on the polarimetric SAR observations, PD theorems have the advantage of removing, up to some extent, the vegetation component [5], [15]–[18]. Hence, combined with PD methods, the empirical (e.g., Oh and Dubois) and physical (e.g., IEM and AIEM) scattering models could be used to estimate the SSM from the remaining ground

scattering components [19], [20]. Notably, the complexity of the volume scattering model [4], [5] and the number of modeled scattering components are important aspects in the description of the scattering properties of this type of scenes. Another strategy to take into account the presence of vegetation on the ground consists in adopting statistical approaches, for instance based on Bayes theorem or on machine learning methods [11], [12], [21]. Artificial neural networks and supported vector regressions have reported some capability to minimize the retrieval uncertainties induced by multiple combinations of surface parameters and improve the inversion of SSM from SAR data [13], [22], [23]. Their effectiveness was also confirmed by combining them with vegetation information derived from optical remote sensing (e.g., vegetation indices) [24], [25]. However, these approaches need extensive reference datasets (SAR, optical, and *in situ* observations) for training the SSM retrieval models.

The change detection-based method, also known as alpha approximation method [10], [14], exploits frequent repeat SAR observations to minimise the influence of crop type and the demand of ancillary information. It is constructed under the assumption of time-invariant roughness and vegetation conditions [14]. Several works have reported the potential of such a method in SSM estimation by utilizing time series of RADARSAT-2, Sentinel-1, ALOS/PALSAR-1 data, yielding a final root-mean-square error (rmse) around 5.0%–7.0% cm^3/cm^3 [3], [26], [27]. However, there are still some limitations in the alpha approximation method—namely, the sensitivity to the initial estimation of the bounds of the soil dielectric constant, and the neglecting of multiple scattering components from vegetation, particularly in the case of dense crop canopies. Besides, this method results in an ill-posed numerical problem which is expected to be circumvented with multi-incidence, multipolarization, and multifrequency SAR observations [2], [26], [28].

The main purpose of this work is to study the potential improvement of the alpha approximation method in SSM estimation over agricultural fields by means of the exploitation of PD theorems and multi-incidence observations. In principle, PDs can help to minimise the volume scattering component and, consequently, the resulting HH and VV backscatter coefficients, which are regarded as only related with ground scattering, would be better suited for SSM estimation. On the other hand, the joint usage of data acquired at multiple incidence angles allows us to increase the observation space because additional sources of information are added. Time series of the soil dielectric constant are calculated by solving a modified underdetermined linear least square system and then converted into volumetric soil moisture values. The extended algorithm was applied to the uninhabited aerial vehicle synthetic aperture radar (UAVSAR) *L*-band data acquired during the Soil Moisture Active Passive Validation Experiment in 2012 (SMAPVEX12). The retrieval performance was assessed by comparing the inversion results with *in situ* measurements over bean, canola, corn, soybean, and wheat areas.

The article is organized as follows. Section II describes the airborne UAVSAR datasets and the selected study area. Section III presents the extended multi-incidence alpha approximation method, PD model, and the generation of soil dielectric constant constraints. The experimental results are shown and discussed in Section IV. Conclusions are presented in Section V.

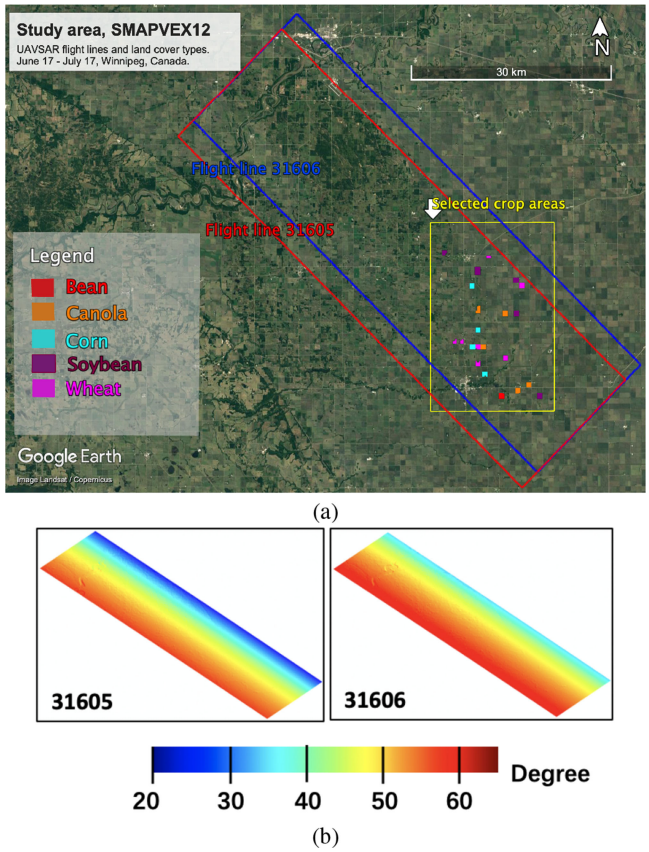

Fig. 1. Selected study crop areas in Winnipeg, Manitoba, Canada. (a) Study area and flight lines. (b) Incidence angle of the overlapping area of flight line #31605 and #31606.

II. Datasets

Time series of UAVSAR data over Winnipeg, Manitoba, Canada were obtained during the SMAP Validation Experiment 2012 (SMAPVEX12) on fourteen dates (see Table I). UAVSAR is a quad polarimetric *L*-band SAR sensor operated at 1.26 GHz. There are four flight lines—namely, #31603, #31604, #31605, and #31606, which were collected over a swath between 20° and 65° on each acquisition date. In this work, flight lines #31605 and #31606 [red and blue rectangle in Fig. 1 (a)] were selected for the multi-incidence alpha approximation SSM estimation method. The incidence angle difference between #31605 and #31606 is about 3° and 12° in the far and near range of the overlapping areas [see Fig. 1 (b)], respectively.

The SAR data were processed by extracting the coherency matrix $T3$ from the calibrated multilooked cross-products with spatial resolution of 5.0 m in the range direction and 7.2 m in the azimuth direction, for which PolSARpro v6.0 (Biomass Edition) was employed. Then, a 7x7 refined Lee filter was used to suppress the speckle noise.

Field survey data including the range of surface roughness, *in situ* measurements of near-surface (0–5 cm) volumetric soil

TABLE I
UAVSAR DATA OF SMAPVEX12 FOR THE WINNIPEG CANADA

Sensor	Flight line	Observation Date (2012)	Incidence angle (°)	Resolution (m)
UAVSAR	#31605, #31606 (of each date)	June 17, 19, 22, 23, 25, 27, 29. July 3, 5, 8, 10, 13, 14, 17. (14 days)	20−65	5.0 (range) × 7.2 (azimuth)

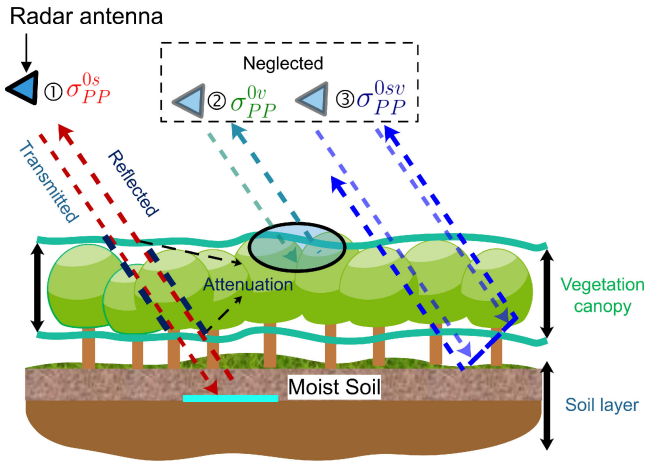

Fig. 2. Radar backscatter measurement over vegetated areas. The volume (dotted green arrow) and double bounce (dotted blue arrows) scattering are negligible in alpha approximation method, and the total backscatter measurement corresponds to the surface scattering (dotted red arrow) attenuated by vegetation canopy.

moisture, and ancillary information, e.g., crop type, height, PWC, etc., were also collected and here are employed in the evaluation of the SSM retrieval performance.

III. METHOD

In order to explain the formulation of the application of PDs and the multi-incidence approach to the alpha approximation method, we first review briefly the original method. Then the proposed modifications are described.

A. Original Alpha Approximation for SSM Estimation

In general, the copolarized (HH and VV) total backscatter coefficient can be expressed as the sum of surface, volume, and double bounce contributions, as shown in Fig. 2 and as follows:

$$\sigma^{0}_{PP} = \sigma^{0s}_{PP} \cdot \exp(-\tau) + \sigma^{0v}_{PP} + \sigma^{0sv}_{PP} \tag{1}$$

where PP denotes the polarization channel, i.e., HH or VV.

In the alpha approximation method, the volume and double bounce contributions, i.e., σ^{0v}_{PP} and σ^{0sv}_{PP}, are considered negligible. Consequently, the total backscatter measurement (σ^{0}_{PP}) corresponds to the surface scattering component (σ^{0s}_{PP}) attenuated by the vegetation canopy ($\exp -(\tau)$).

Assuming that no variation of vegetation condition and surface roughness happens between two consecutive SAR measurements, the change between the two backscatter measurements depends only on soil moisture and incidence angle. Therefore, the ratio of two copolarized radar backscatter measurements is approximately equal to the squared ratio of alpha coefficients

$$\frac{\sigma^{0\_tj}_{PP}}{\sigma^{0\_ti}_{PP}} = \left|\frac{\alpha^{tj}_{PP}(\varepsilon,\theta)}{\alpha^{ti}_{PP}(\varepsilon,\theta)}\right|^2 \tag{2}$$

where $\sigma^{0\_ti}_{PP}$ and $\sigma^{0\_tj}_{PP}$ are the backscatter coefficient measured at dates ti and tj, respectively. The alpha coefficient is a function of incidence angle (θ) and soil dielectric constant (ε), as shown in

$$\begin{aligned}\alpha_{HH} &= \frac{(\varepsilon-1)}{\left[\cos\theta + \sqrt{\varepsilon - \sin^2\theta}\right]^2} \\ \alpha_{VV} &= \frac{(\varepsilon-1)\left[\sin^2\theta - \varepsilon(1+\sin^2\theta)\right]}{\left[\cos\theta + \sqrt{\varepsilon - \sin^2\theta}\right]^2}.\end{aligned} \tag{3}$$

For a time series of N single-incidence SAR observations, the corresponding matrix equation to be solved is given as

$$M^{\theta_1}_{PP} \cdot A^{\theta_1}_{PP} = \begin{bmatrix}0 & 0 & 0 & \cdots & 0\end{bmatrix}^T_{N-1} \tag{4}$$

where T denotes the transpose, and

$$M^{\theta_1}_{PP} = \begin{bmatrix} 1 & -\sqrt{\frac{\sigma^{0\_t1}_{PP}}{\sigma^{0\_t2}_{PP}}} & 0 & \cdots & 0 & 0 \\ 0 & 1 & -\sqrt{\frac{\sigma^{0\_t2}_{PP}}{\sigma^{0\_t3}_{PP}}} & \cdots & 0 & 0 \\ \vdots & \vdots & \vdots & \vdots & \vdots & \vdots \\ 0 & 0 & 0 & 0 & 1 & -\sqrt{\frac{\sigma^{0\_t(N-1)}_{PP}}{\sigma^{0\_t(N)}_{PP}}} \end{bmatrix} \tag{5}$$

is an $(N-1)\times N$ matrix, and the unknowns form a vector of size N

$$A^{\theta_1}_{PP} = \begin{bmatrix}|\alpha^{t1}_{PP}| & |\alpha^{t2}_{PP}| & \cdots & |\alpha^{tN}_{PP}|\end{bmatrix}^T_N. \tag{6}$$

In (4), the number of unknown soil dielectric constants (N) is larger than the observation equations (N-1), hence, the soil moisture retrieval is expressed as an underdetermined problem which is usually solved by employing a bounded linear least-squares optimization [27]. Once the α_{PP} values in (6) have been estimated, the complex-valued dielectric constant is inverted for each observation and mapped to soil moisture content using a dielectric mixing model [29].

B. Introduction of a PD in the Alpha Soil Moisture Estimation

The formulation reviewed in the previous subsection is valid for any of the two co-polar backscattering coefficients, i.e., HH or VV, since there exists a way to link them to the soil

dielectric constant. In fact, the two channels can be used jointly in the estimation, as it was demonstrated in [26], improving the retrieval performance in some cases. In this work, we propose an alternative way to exploit polarimetry for improving the performance of the alpha method. The idea consists in applying a PD scheme to isolate, or separate in a better way, the radar response of the ground from that of the vegetation. In this way, we expect the relationship between radar data and soil moisture to be less affected by the presence of vegetation.

Model-based PD techniques are commonly used for trying to separate the contributions of vegetation and ground from the observed backscattered signal [30]–[32]. This approach was also applied to soil moisture estimation combined with some physical and semiempirical models [15], [16]. Here we make use of a recent approach in which a two-component decomposition technique [20] was employed to extract the HH and VV backscatter components that are relevant to the soil scattering for the SSM estimation. Under reflection symmetry assumption, the two-component decomposition model can be expressed as in

$$T_3 = T_G + T_V = \begin{bmatrix} T_{11} & T_{12} & 0 \\ T_{12}^* & T_{22} & 0 \\ 0 & 0 & T_{33} \end{bmatrix} \tag{7}$$

where T_3 is the total coherency matrix of quad polarized SAR observations, T_G represents the ground scattering contribution, which is usually expressed using the X-Bragg model, and T_V corresponds to the volume scattering component, which includes three types of vegetation orientation distributions: random, vertical, and horizontal. In this method, T_V is estimated and removed from the total backscatter on the basis of the nonnegative eigenvalue decomposition concept, and the ground scattering coefficients at HH and VV are obtained using the unitary transformation between the coherency and covariance matrices of the ground, as shown in

$$\begin{aligned} \sigma_{HH}^0 &= (T_{G11} + T_{G12} + T_{G12}^* + T_{G22})/2 \\ \sigma_{VV}^0 &= (T_{G11} - T_{G12} - T_{G12}^* + T_{G22})/2 \end{aligned} \tag{8}$$

where T_{G11}, T_{G12}, T_{G22} are the elements of T_G, and $*$ denotes complex conjugation. Consequently, the extracted ground scattering coefficients at HH and VV are used as inputs for the alpha estimation method in this work.

C. Multi-Incidence Extension

As it was shown in [26], the use of more than one channel of information is beneficial for the SSM inversion algorithm although the undetermination of the equation system is maintained. In that work, the alpha approximation SSM retrieval method was extended to multiple polarizations, i.e., combining HH and VV observations acquired at the same incidence angle ($\theta_1 = \theta_2$). An alternative way to provide extra information channels consists in incorporating multi-incidence SAR observations. As illustrated in Fig. 3, the theoretical alpha coefficients of HH and VV are sensitive to both incidence angle and soil dielectric constant. Particularly, the alpha coefficient at the VV channel is more sensitive to the incidence angle than that at the HH channel. The

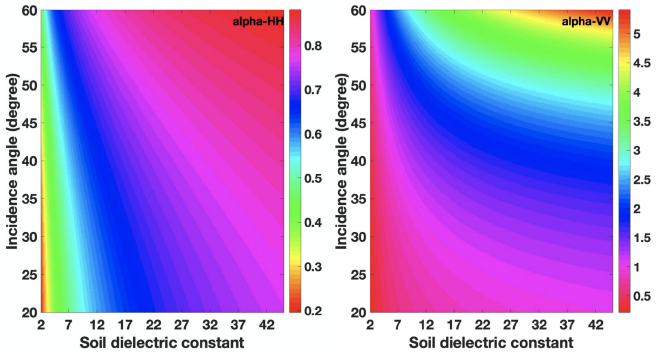

Fig. 3. Sensitivity of alpha coefficient at HH and VV channels to the incidence angle and soil dielectric constant.

resulting equation system with multi-incidence SAR observations is the following one:

$$\begin{bmatrix} M_{PP}^{\theta_1} & M_0 \\ M_0 & M_{PP}^{\theta_2} \end{bmatrix} \cdot A_{PP}^{\theta_1\_\theta_2} = \begin{bmatrix} 0 & 0 & 0 & \cdots & 0 \end{bmatrix}_{2(N-1)}^T \tag{9}$$

where $M_{PP}^{\theta_1}$ and $M_{PP}^{\theta_2}$ are the matrices obtained from the SAR backscatter measurements acquired with incidences θ_1 and θ_2, respectively. M_0 is a $(N-1) \times N$ null matrix, and $A_{PP}^{\theta_1\_\theta_2}$ is the vector of multi-incidence alpha coefficients, given as

$$A_{PP}^{\theta_1\_\theta_2} = \begin{bmatrix} \left|\alpha_{PP}^{t1\_\theta_1}\right| & \cdots & \left|\alpha_{PP}^{tN\_\theta_1}\right| & \left|\alpha_{PP}^{t1\_\theta_2}\right| & \cdots & \left|\alpha_{PP}^{tN\_\theta_2}\right| \end{bmatrix}_{2N}^T. \tag{10}$$

After the equation system in (9) is solved, the soil dielectric constant is retrieved individually for the two polarization channels (HH and VV), hence providing two separate SSM estimates.

Alternatively, as it was done in the multipolarization retrieval algorithm proposed in [26], the soil dielectric constant could be calculated from a joint cost function which simultaneously exploits the alpha coefficients found for both polarizations. For instance, (11) was employed in [26] to retrieve the soil dielectric constant from the derived alpha values, i.e., α_{HH} and α_{VV}, and the lookup tables, i.e., α_{HH_Lut} and α_{VV_Lut}. The difference between the multipolarized alpha approximation method introduced in [26] and the multi-incidence retrieval approach proposed in this work is that the latter one extends the observation matrix with observations at different incidence angles rather than different polarizations. The multipolarization approach (denoted as MPAP), in which (11) is employed for the inversion, is compared in the Results section with the algorithms proposed in this work

$$cost\_fun = Min\left| |\alpha_{HH} - \alpha_{HH\_Lut}|^2 + |\alpha_{VV} - \alpha_{VV\_Lut}|^2 \right| \tag{11}$$

Finally, all retrieval methods in this work are applied to the time-series UAVSAR data set (14 dates, 28 PolSAR images) using a scheme similar to that employed in [26]: a sliding window of four UAVSAR measurements to provide SM estimates at every day in the observation period, for which the average value of the estimations is considered for validation and analysis.

D. Soil Dielectric Constant Bounds Conditions

In addition to the two previous extensions of the alpha model, we also include here a modification in the way the bound conditions of the soil dielectric constant are defined. These bound conditions are required for the inversion of the equation system defined in (4) or (9) [27]. Dubois proposed a semiempirical model to estimate the copolarized backscattering coefficient in HH (σ^0_{HH}) polarization and VV polarization (σ^0_{VV}) over bare soils [33]. This model is constructed as a function of the dielectric constant (ε), root-mean-square height (s) of the surface, incidence angle (θ), and wavelength (λ), resulting in the following expressions:

$$\sigma^0_{HH} = 10^{-2.75}\left(\frac{\cos^{1.5}\theta}{\sin^5\theta}\right)10^{0.028\varepsilon\tan\theta}(ks\cdot\sin\theta)^{1.4}\lambda^{0.7}$$
$$\sigma^0_{VV} = 10^{-2.35}\left(\frac{\cos^{1.5}\theta}{\sin^5\theta}\right)10^{0.046\varepsilon\tan\theta}(ks\cdot\sin\theta)^{1.1}\lambda^{0.7} \tag{12}$$

where k is the wavenumber ($k = 2\pi/\lambda$). The empirical parameters in (12) are derived from Michigan's LCX POLARSCAT truck-mounted scatterometer dataset (operating at 1.25, 4.75, and 9.5 GHz), and the University of Berne's RASAM truck-mounted scatterometer dataset (operating at six frequencies between 2.5 and 11 GHz) [33]. It requires the two copolarized channels at a frequency between 1.25 and 11 GHz and has the best performance for $ks \leq 2.5$, $mv \leq 35\%$, and $\theta \geq 30^\circ$ over bare surfaces. Since the Dubois model provides a simple relationship between radar signal and soil parameters, the present study employs (12) and a lookup table to determine the bound conditions of the soil dielectric constant.

Fig. 4 illustrates the method for determining these bounds with the *priori* knowledge of the surface roughness and the time series of SAR observations. The upper bound is derived from the minimum backscattering coefficient and maximum root mean square height, whereas the lower bound is derived from maximum backscattering coefficient and minimum root mean square height. The typical range of the root mean square height and the soil dielectric constant are selected as $0.3 \leq s \leq 10.0$ cm and $4 \leq \varepsilon \leq 35$, respectively. It should be noted that the empirical Oh model [34] could also be used to determine the soil dielectric constant bound conditions [3]. However, considering that the validity of Oh model was tested over ranges of $0.39 \leq s \leq 22.72$ cm and $9.0\% \leq mv \leq 31.0\%$, which are beyond the range of the soil conditions of the study areas, Dubois model is more appropriate for this case study.

The whole algorithm that includes the proposed modifications or extensions is illustrated in Fig. 5.

IV. Results

A. Constraints of Soil Dielectric Constant

Fig. 6 presents the upper and lower bounds of the soil dielectric constant derived from the original backscatter measurements and from the inclusion of the PD as introduced in Section III. It shows that the effective range of soil dielectric constant is refined, as expected, since it is narrower than the typical bounds

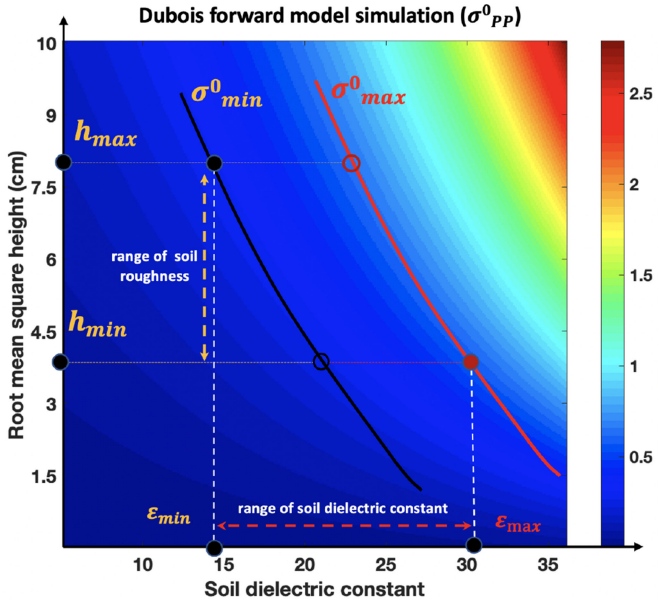

Fig. 4. Relationship between backscattering coefficient, soil surface roughness, and the bound conditions of soil dielectric constant. σ^0_{PP} represent the backscattering coefficient of HH or VV polarization, σ^0_{min} and σ^0_{max} denote the minimum and maximum backscattering coefficient of the time series observations, respectively. h_{min} and h_{max} represent the minimum and maximum soil surface roughness provided by the field surveying (prior knowledge). ε_{min} and ε_{max} are the determined minimum and maximum soil dielectric constant, respectively.

(0–35). The calculated constraints of HH and VV channels are different over different fields because of the knowledge of the surface roughness. Theoretically, the derived constraints of the dielectric constant is dependent upon the range of the time series of backscatter measurements and independent of the polarizations. However, under the presence of a vegetation canopy and due to the evolution of the crop phenology, the attenuation of the backscatter power is different for both HH and VV channels. As a result, the derived bound conditions of dielectric constant are different for HH and VV. Since the solution of (9) is sensitive to the constraints of ε, the narrower the bound conditions, the less uncertainty in the final retrieval results. Nevertheless, although the intervals of ε obtained with the PD are narrower than the original ones, they show no significant difference when compared with those obtained from the original backscatter measurements at HH and VV polarization channels.

B. Soil Moisture Estimation Over Agricultural Fields

In order to get a first insight on the expected results, Fig. 7 shows the time series of SSM estimates obtained by the original alpha approximation method (OAP) and by the method extended with both the PD and the multi-incidence data (PDMIAP). The estimates are compared against the *in situ* measurements over individual fields of bean, canola, corn, soybean, and wheat. It should be noted that the SSM estimates which are compared against *in situ* measurements are the average value of a region of pixels around the field acquisition locations. These regions were selected manually attending to the particular shape of the

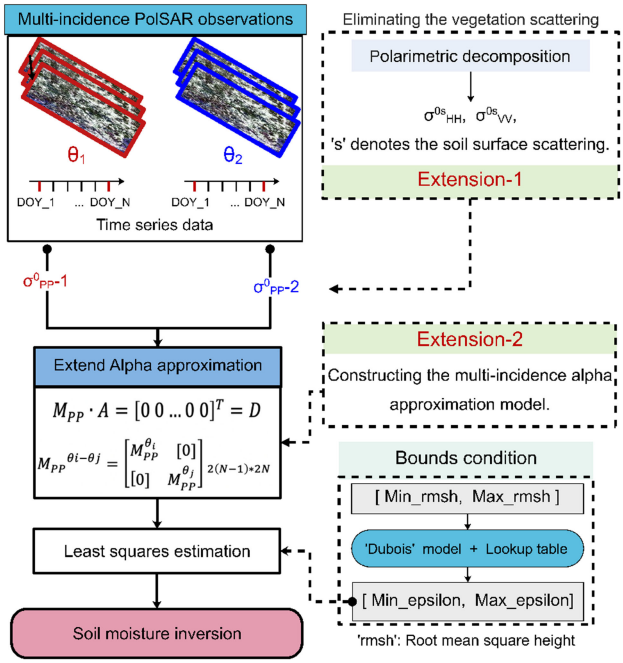

Fig. 5. Alpha approximation for SSM inversion extended with multi-incidence observations and a PD technique.

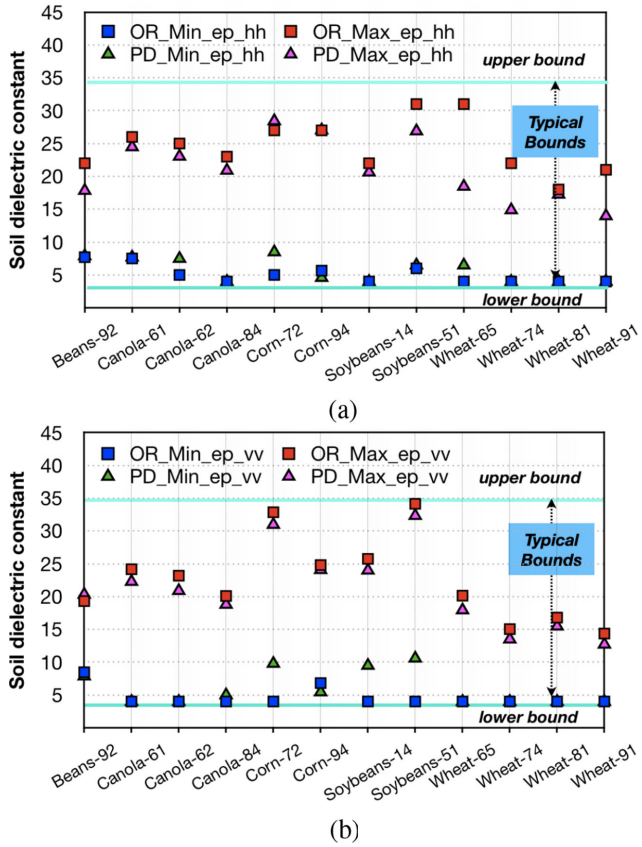

Fig. 6. Soil dielectric constant bound conditions derived by Dubois model from time series HH and VV observations. The green ("OR_Min_ep_hh/vv") and pink ("OR_Max_ep_hh/vv") squares correspond to the minimum and maximum ε derived from original observations, respectively. The triangles in green ("PD_Min_ep_hh/vv") and pink ("PD_Max_ep_hh/vv") correspond to the minimum and maximum ε derived from the backscatter values after the PD, respectively. The light green horizontal lines denote the typical bounds. (a) Bound conditions calculated for HH. (b) Bound conditions calculated for VV.

fields (elongated in N–S or E–W direction) and include between 190 and 320 pixels. Both the OAP and PDMIAP algorithms exhibit some potential of SSM estimation over vegetated areas. Although the total dynamic range of SSM is low (less than 10% excursion was observed in the crop locations), the retrieved values capture in some cases the temporal evolution of the actual SSM. A visual comparison of both columns of Fig. 7 reveals that the largest improvement from OAP (left) to PDMIAP (right) is obtained for the wheat fields, followed by corn and soybeans, and there does not seem to be much improvement for the fields of canola and bean.

A complete quantitative assessment of the results provided by the different approaches is illustrated in Table III, in which the mean average error (MAE), the rmse, and the correlation coefficient (R) of the SSM estimates are obtained for all fields of each crop type. Besides the OAP and the PDMIAP methods, we have also tested the inclusion of the PD (without multi-incidence data), the multi-incidence data (without PD), and the multipolarized data (without PD) in the alpha method alone, hereafter denoted as PDOAP, MIAP, and MPAP, respectively.

1) Retrieval Performance of Different Methods: Figs. 8 and 9 show the scatterplots of the retrieval results from different methods for the five crop types one by one. Among the five methods, PDMIAP estimates are more consistent with the *in situ* measurements. In Fig. 9 (b), the dots are scattered more close to the red dotted lines compared with the retrieval results of the other four approaches. As also seen in Table III, over corn, soybean and wheat, the rmses for HH and VV are both decreased with PDMIAP benefiting from the PD and the incorporation of multi-incidence observations. In particular for wheat, the PDMIAP estimates show the absolute highest accuracy of rmse $= 3.2\%$ (HH) and rmse $= 3.7\%$ (VV) which also fulfill the SMAP mission requirement: rmse ≤ 0.04 m^3·m^{-3}.

However, there is no improvement in SSM estimation by MIAP, except for corn. For bean, canola, soybean and wheat, an increase of rmses is found with MIAP at both HH and VV channels. For instance, over soybean fields the rmse increases from 6.3% to 9.4% at HH and from 5.9% to 9.0% at VV, respectively. These unexpected results are also provided by the MPAP. As illustrated in Fig. 8 (c) and Table III, the apparent overestimation of SSM is found for the overall five crop types and the retrieval accuracy is more degraded relative to the performance of OAP at VV channel. It seems that, without adding the PD, the usage of two incidences or polarization channels does not work well for the SSM estimation due to the error induced by the volume scattering contribution in the additional observations.

To have an overall view of the performance of different methods, Fig. 10 shows the correlation and rmse obtained for the whole set of data, formed by all the fields of the five crop types, by the OAP, MIAP, PDOAP, and PDMIAP methods at HH and VV channels. Compared with the OAP method, a similar retrieval accuracy is provided by the MIAP with an rmse of

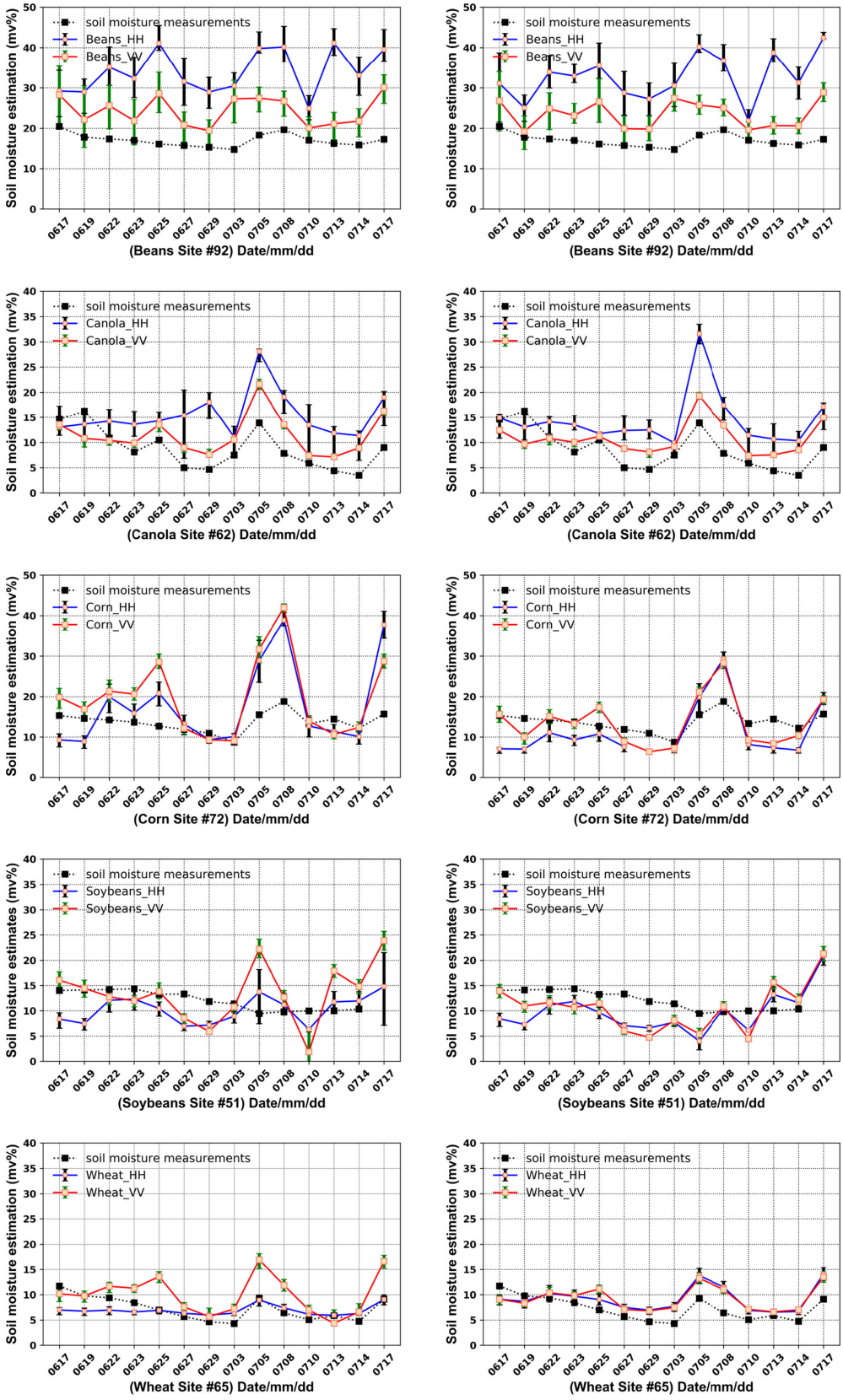

(a) OAP (b) PDMIAP

Fig. 7. Time series of the *in situ* SM measurements (dotted black line) and the estimates from HH (blue line) and VV (red line) channels observations over individual fields of bean, canola, corn, soybean, and wheat. (a) OAP method. (b) PDMIAP method.

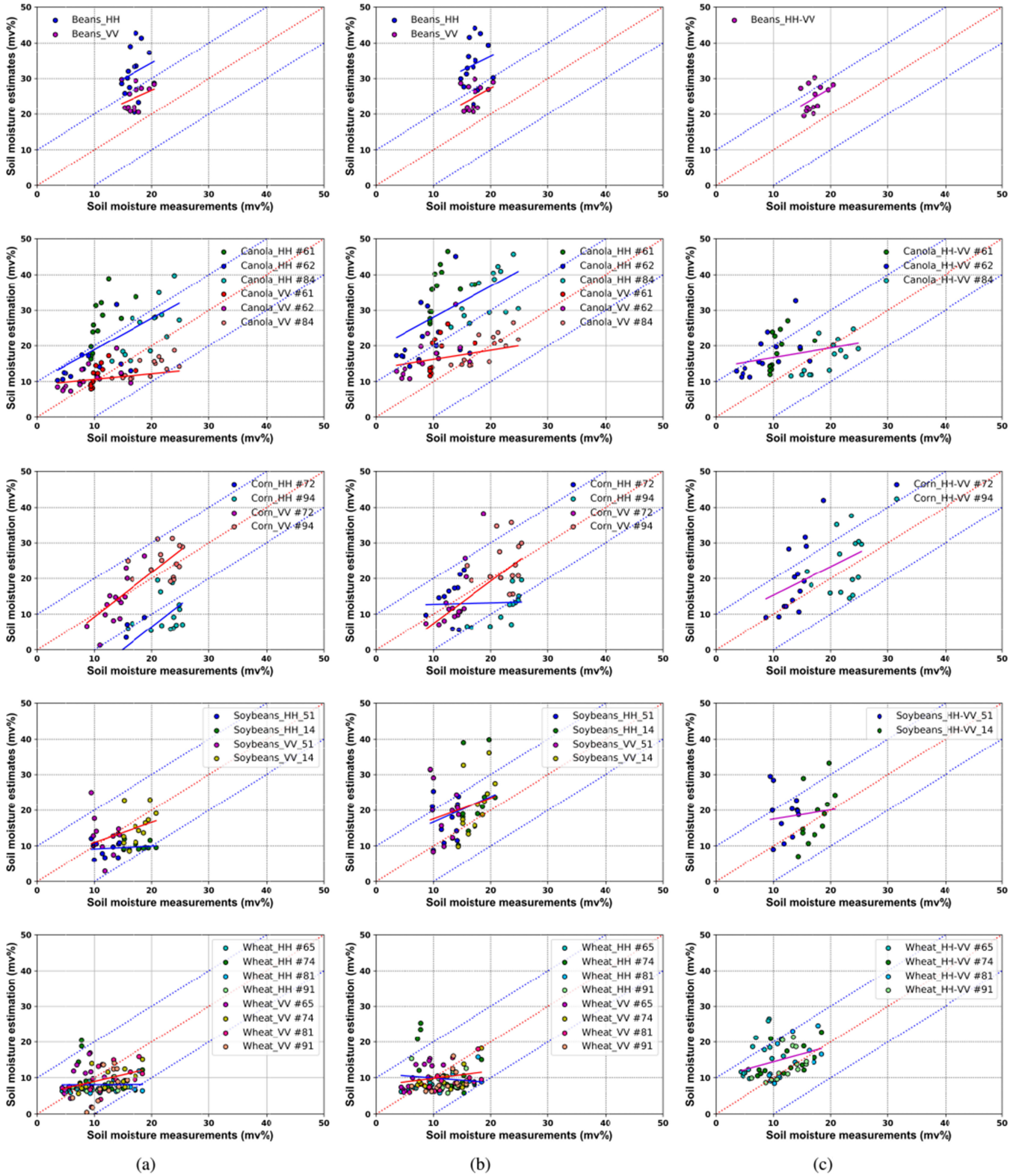

Fig. 8. Scatterplots of *in situ* measurements and SSM estimates from OAP, MIAP, and MPAP methods over bean, canola, corn, soybean, and wheat fields. (a) OAP. (b) MIAP. (c) MPAP method. The blue, red, and pink solid lines denote the linear correlation between the *in situ* measurements and estimates.

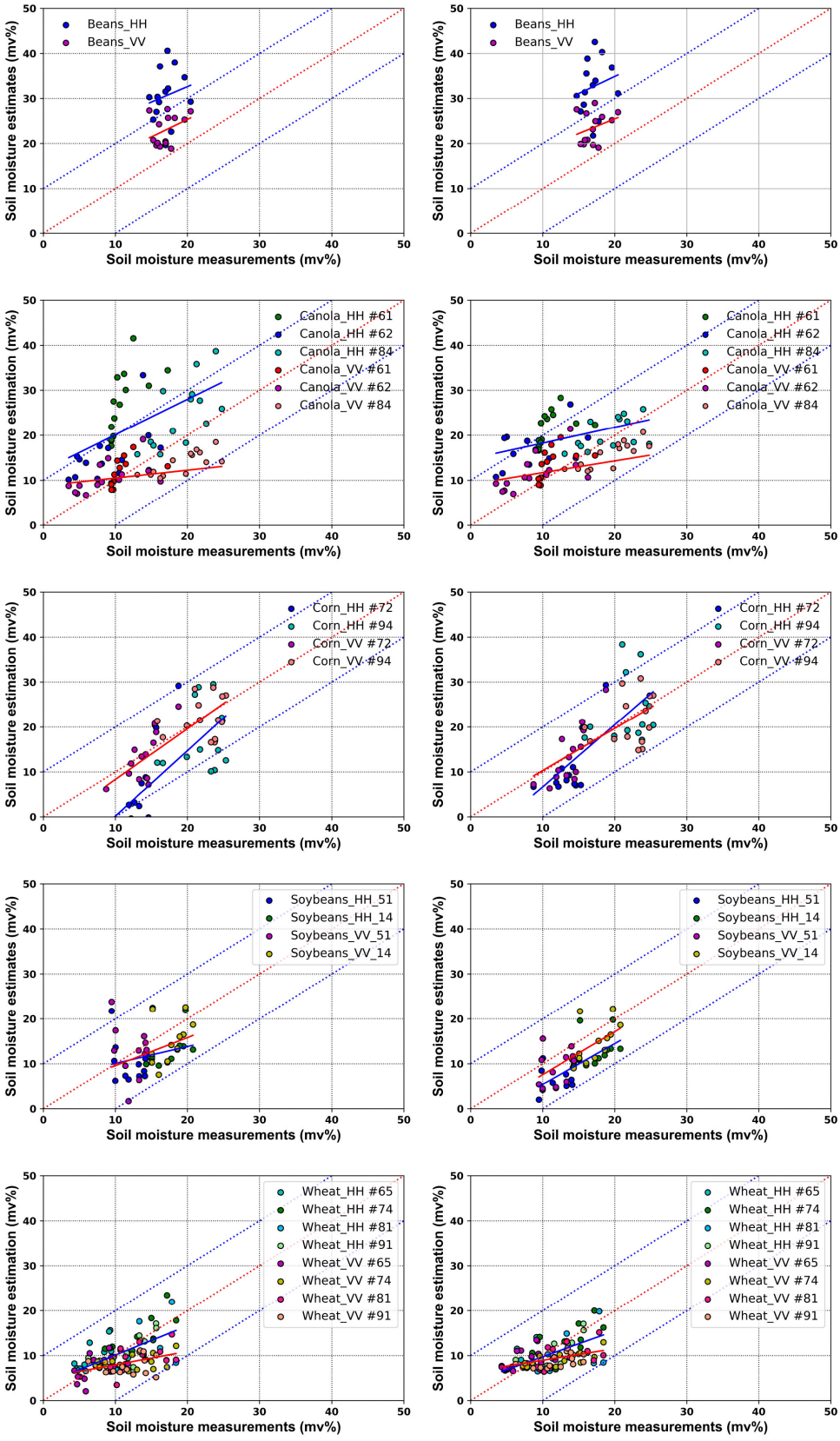

Fig. 9. Scatterplots of *in situ* measurements and SSM estimates from PDOAP and PDMIAP methods over bean, canola, corn, soybean, and wheat fields. (a) PDOAP method. (b) PDMIAP method. The blue and red solid lines denote the linear correlation between the *in situ* measurements and estimates.

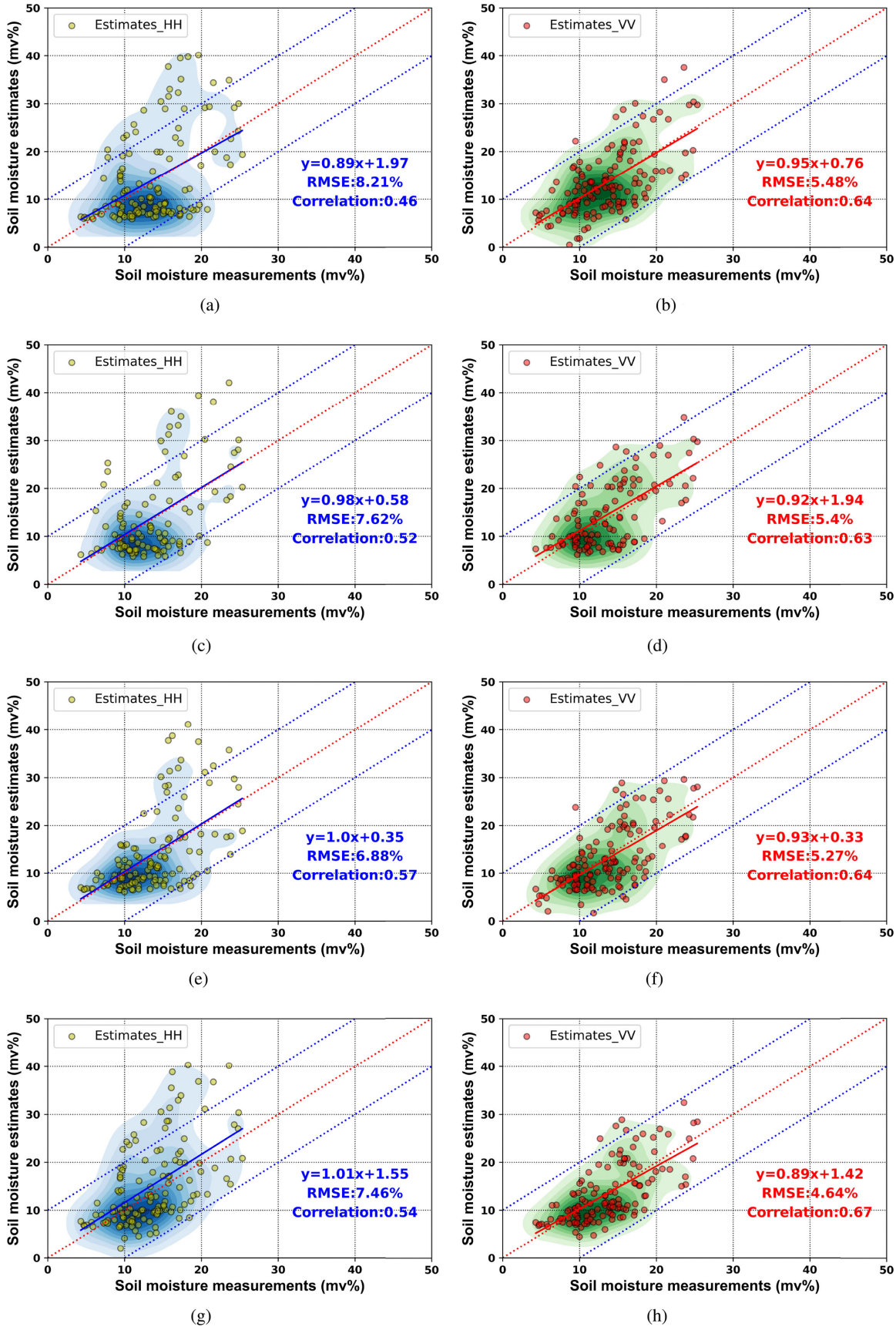

Fig. 10. Scatterplots of the *in situ* SSM measurements and estimates from HH (green) and VV (red) observations by OAP, MIAP, PDOAP, and PDMIAP algorithms. (a) OAP-HH. (b) OAP-VV. (c) MIAP-HH. (d) MIAP-VV. (e) PDOAP-HH. (f) PDOAP-VV. (g) PDMIAP-HH. (h) PDMIAP-VV.

TABLE II
SURFACE ROUGHNESS INFORMATION

Crop type	Min-RMSH (cm)	Max-RMSH (cm)
Bean	0.62	0.90
Canola	0.69	1.71
Corn	0.60	1.89
Soybean	0.34	1.89
Wheat	0.44	1.26

"Min-RMSH" and "Max-RMSH" are the minimum and maximum root-mean-square height of the soil surface, respectively.

TABLE III
RETRIEVAL ACCURACY OF OAP, MIAP, MPAP, PDOAP, AND PDMIAP ALGORITHMS

Method	MAE		RMSE		R	
	HH	VV	HH	VV	HH	VV
Bean						
OAP	14.7	7.2	15.9	7.8	0.41	0.43
MIAP	16.8	7.6	17.9	8.3	0.20	0.40
MPAP	7.5		8.1		0.42	
PDOAP	13.6	6.3	14.7	7.3	0.24	0.22
PDMIAP	15.6	6.4	16.5	7.1	0.22	0.30
Canola						
OAP	17.3	6.2	18.9	7.4	0.25	0.23
MIAP	17.6	6.1	19.3	7.3	0.24	0.23
MPAP	6.4		7.8		0.22	
PDOAP	10.0	5.9	12.6	6.9	0.32	0.22
PDMIAP	11.3	5.8	13.7	6.8	0.29	0.22
Corn						
OAP	10.4	6.0	11.8	7.1	0.72	0.81
MIAP	7.9	4.0	8.9	4.9	0.04	0.80
MPAP	6.7		8.7		0.45	
PDOAP	10.2	5.8	11.6	7.1	0.63	0.82
PDMIAP	5.2	4.0	6.5	4.9	0.71	0.73
Soybean						
OAP	5.5	4.5	6.3	5.9	0.17	0.32
MIAP	6.4	6.7	9.4	9.0	0.29	0.27
MPAP	6.0		8.1		0.13	
PDOAP	5.1	5.3	5.6	6.8	0.27	0.30
PDMIAP	5.9	3.9	5.9	4.4	0.69	0.67
Wheat						
OAP	4.5	3.8	5.6	4.5	0.01	0.38
MIAP	4.9	3.7	6.3	4.4	-0.1	0.23
MPAP	4.7		6.3		0.34	
PDOAP	2.6	4.2	3.3	5.0	0.60	0.35
PDMIAP	2.5	3.1	3.2	3.7	0.62	0.48

7.62% at HH and 5.4% at VV, respectively. The improvement in SSM estimation by PDOAP, particularly at HH, could also be observed in Fig. 10(e) and (f) as well as in Fig. 9(a) and Table III. For example, the retrieval accuracy of PDOAP at HH is decreased by 6.3% and 2.3% for canola and wheat, respectively. Considering the five crop types, with the inclusion of both the PD and the multi-incidence observations, the total rmse of PDMIAP estimates at HH and VV is decreased by 0.75% [see Fig. 10 (g)] and 0.84% [see Fig. 10 (h)], respectively. It means that the overall best results are obtained with the PDMIAP method. In particular, the PDMIAP applied on VV backscatters shows the best performance in SSM retrieval.

Low correlation ($R \leq 0.5$) between the estimates of OAP and *in situ* measurements is observed for all crops, especially over bean and canola. However, over corn, soybean, and wheat fields, the results of the PDMIAP approach show a moderate correlation, i.e., larger than 0.6, with the *in situ* data. This performance is better described with the values in Table III. In the corn case, the proposed extensions of the alpha method improve notably the rmse, whereas the correlation is similar to that of the OAP. Contrarily, for wheat the correlation is clearly improved with PDMIAP, especially at the HH channel, and the rmse is also improved despite it presented the best results with OAP among all the crops studied here.

2) Retrieval Performance With HH and VV Channels: For bean, canola, and corn, the rmse of the original HH-derived estimates (OAP) is larger than 10%, which shows a weak sensitivity to SSM. In contrast, the results obtained for VV data present a promising starting accuracy for these crop types, with rmse less than or equal to 7% with the original approach (OAP). For soybean and wheat, a similar retrieval accuracy is observed for both HH and VV, which is better than for bean, canola, and corn. In particular, the performance over wheat areas is the best, with an rmse lower than 6.0% in all cases.

The contribution of adding the polarimetric decomposition (PDOAP) and also the multi-incidence data (PDMIAP) is different for the five crop types considered in this study. For bean and canola, the improvement in the SSM estimates is limited. At the VV channel, the rmse is improved less than 1% when compared to OAP. In the case of the HH polarization, there is a clear improvement for canola, especially with the PDOAP method, since the rmse decreases from 18.9% to 12.6%. However, the final rmse values at the HH channel are still very high for canola and bean. A very different behaviour is found at the corn fields, for which the improvement is notable, especially with the PDMIAP method: the rmse decreases from 11.8% to 6.5% at HH and from 7.1% to 4.9% at VV channel. These numbers demonstrate the contribution of the proposed extension of the alpha method, since corn is known to be not well adapted to the original alpha method because of the important backscatter from the vegetation volume. For soybean there is few improvement at HH, but it is clear at the VV channel, with rmse decreasing from 5.9% with OAP to 4.4% with PDMIAP. Finally, despite it started with the best results of the OAP method, a clear improvement in SSM estimation is obtained in the wheat fields, by PDOAP at HH and by both PDOAP and PDMIAP at VV.

3) Comparison of Results With Previous Studies: The same UAVSAR dataset has been exploited with other SSM retrieval algorithms in a set of fields of the SMAPVEX12 campaign. In [26], ground-sampled SSM data were used to constrain the alpha coefficient for the time-series retrieval. Their results show a total accuracy of 6.9% for HH and 6.1% for VV polarization over canola, corn, and wheat fields. In [35], SSM estimates

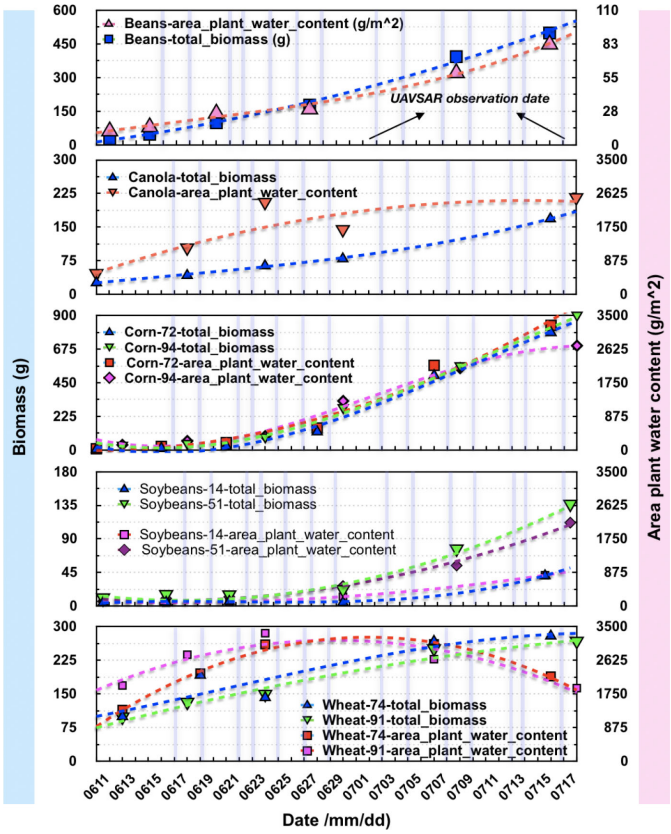

Fig. 11. Evolution of crop total biomass and PWC over bean, canola, corn, soybean, and wheat fields during the SMAPVEX12 campaign.

from a data-cube time-series method, combined with HH and VV measurements, provided rmse values of 5.0%, 7.1%, and 9.0% for wheat, corn, and bean, respectively. Besides, as shown in [5], [36], [37] PD was applied to SSM estimation, in which the soil permittivity was retrieved by minimizing the cost functions between observations and forward scattering models of surface and dihedral components. The rmse of SSM estimates ranged from 6.1% to 12.0% for canola, corn, and wheat, depending on the crop types and vegetation characteristics. Comparing our results (i.e., rmses between 3.7% and 7.1%) with the outcomes of these studies, the inclusion of multi-incidence observations, PD technique, and the bound conditions of dielectric constant in the alpha approximation method provide some improvement in SSM estimation over the selected crop fields.

V. Conclusion

This work proposes an extended alpha approximation method for SSM estimation over agricultural areas by incorporating multi-incidence data, to enlarge the observation space, and a PD approach, to separate in a better way the response of the ground from that of the vegetation. The proposed method was applied to *L*-band UAVSAR data acquired during the SMAPVEX12 campaign over bean, canola, corn, soybean, and wheat fields. The SSM estimates were compared against the *in situ* measurements at a depth of 5 cm from the surface.

Results show that, compared with the original method, the retrieval accuracy is improved when the PD is included in the approach. However, no improvement was found with the inclusion of multiple incidences or polarization channels (without polarimetric decomposition). With the proposed approach, which combines both the polarimetric decomposition and multi-incidence observations, the rmse values decrease by 0.4%–5% and 0.6%–2% for the HH and VV channels, respectively, depending on the crop type. The improvement is very clear for corn, soybean and wheat, hence demonstrating the contribution of this extension of the alpha method. It is also found that the SSM estimation at VV channel is better than at the HH channel, which can be justified by the stronger backscatter at VV than at HH from soil surfaces. Notwithstanding the accuracy of SSM retrieval over vegetation areas could be improved by the proposed approach, it still does not match the standard requirement of satellite SSM products (rmse ≤ 0.04 $m^3 \cdot m^{-3}$).

In comparison to data-cube time series [35] and PD-based [5], [35]–[37] SSM retrieval methods applied to the same datasets, combining multi-incidence observations and polarimetric decomposition technique with alpha approximation method provides a better accuracy over the selected crop fields. On the one hand, although multiple polarization observations are included in the data-cube time series algorithm, it neglects the multiple scattering between vegetation and soil surface. On the other hand, the PD-based method has the advantage in removing the volume scattering for SSM retrieval. However, it does not make use of the time series information. Since the SSM retrieval estimation is inevitably influenced by crop structure, biomass, PWC, and phenological stage, the elimination of volume scattering needs to be handled properly when adding radar observations for SSM estimation. As shown in Fig. 11, the biomass and the PWC change greatly with the crop types and growth stages. For instance, the PWC ranges from 0 to 110 g/m^2 at beginning and the end of the campaign over bean field, while from 0 to 3500 g/m^2 for corn. Therefore, the feasibility and necessity of combining the alpha method with more generalized and accurate polarimetric scattering models, e.g., [38], [39] will be investigated in the future. In addition, further tests in other locations, with crop types, and at different bands (e.g., at *C*-band) will also be carried out.

Acknowledgment

The authors would like to thank the National Snow and Ice Data Center (NSIDC), NASA, and the SMAPVEX12 funding agencies in Canada and the United States for providing the UAVSAR datasets.

References

[1] F. Lei *et al.*, "Data assimilation of high-resolution thermal and radar remote sensing retrievals for soil moisture monitoring in a drip-irrigated vineyard," *Remote Sens. Environ.*, vol. 239, 2020, Art. no. 111622.

[2] L. Zhu, J. P. Walker, L. Tsang, H. Huang, N. Ye, and C. Rüdiger, "A multi-frequency framework for soil moisture retrieval from time series radar data," *Remote Sens. Environ.*, vol. 235, 2019, Art. no. 111433.

[3] L. He, Q. Qin, R. Panciera, M. Tanase, J. P. Walker, and Y. Hong, "An Extension of the alpha approximation method for soil moisture estimation using time-series SAR data over bare soil surfaces," *IEEE Geosci. Remote Sens. Lett.*, vol. 14, no. 8, pp. 1328–1332, Aug. 2017.

[4] M. Zribi *et al.*, "Analysis of L-band SAR data for soil moisture estimations over agricultural areas in the tropics," *Remote Sens.*, vol. 11, no. 9, 2019, Art. no. 1122.

[5] H. Wang, R. Magagi, and K. Goita, "Comparison of different polarimetric decompositions for soil moisture retrieval over vegetation covered agricultural area," *Remote Sens. Environ.*, vol. 199, pp. 120–136, 9 2017.
[6] G. Singh and Y. Yamaguchi, "Model-based six-component scattering matrix power decomposition," *IEEE Trans. Geosci. Remote Sens.*, vol. 56, no. 10, pp. 5687–5704, Oct. 2018.
[7] J. D. Ballester-Berman, T. L. Ainsworth, and J. M. Lopez-Sanchez, "On the physical quantitative assessment of model-based PolSAR decompositions," 2020, *arXiv:2001.05872*.
[8] W. Wagner, G. Lemoine, and H. Rott, "A method for estimating soil moisture from ERS scatterometer and soil data," *Remote Sens. Environ.*, vol. 70, no. 2, pp. 191–207, 1999.
[9] A. Balenzano, F. Mattia, G. Satalino, V. Pauwels, and P. Snoeij, "SMOSAR algorithm for soil moisture retrieval using Sentinel-1 data," in *Proc. IEEE Int. Geosci. Remote Sens. Symp.*, 2012, pp. 1200–1203.
[10] B. Bauer-Marschallinger*et al.*, "Toward global soil moisture monitoring with Sentinel-1: Harnessing assets and overcoming obstacles," *IEEE Trans. Geosci. Remote Sens.*, vol. 57, no. 1, pp. 520–539, Jan. 2019.
[11] C. Notarnicola, M. Angiulli, and F. Posa, "Soil moisture retrieval from remotely sensed data: Neural network approach versus Bayesian method," *IEEE Trans. Geosci. Remote Sens.*, vol. 46, no. 2, pp. 547–557, Feb. 2008.
[12] S. Paloscia, S. Pettinato, E. Santi, C. Notarnicola, F. Greifeneder, and G. Cuozzo, "COSMO-SkyMed and radarsat image integration for soil moisture and vegetation biomass monitoring," in *Proc. IEEE Int. Geosci. Remote Sens. Symp*, 2017, pp. 5237–5240.
[13] E. Santi *et al.*, "On The use of machine learning and polarimetry for estimating soil moisture from radarsat imagery over Italian and Canadian test sites," in *Proc. IGARSS IEEE Int. Geosci. Remote Sens. Symp.*, 2019, pp. 5760–5763.
[14] A. Balenzano, F. Mattia, G. Satalino, and M. W. J. Davidson, "Dense temporal series of C- and L-band SAR data for soil moisture retrieval over agricultural crops," *IEEE J. Sel. Topics Appl. Earth Observ. Remote Sens.*, vol. 4, no. 2, pp. 439–450, Jun. 2011.
[15] I. Hajnsek, T. Jagdhuber, H. Schon, and K. P. Papathanassiou, "Potential of estimating soil moisture under vegetation cover by means of PolSAR," *IEEE Trans. Geosci. Remote Sens.*, vol. 47, no. 2, pp. 442–454, Feb. 2009.
[16] T. Jagdhuber, I. Hajnsek, A. Bronstert, and K. P. Papathanassiou, "Soil moisture estimation under low vegetation cover using a multi-angular polarimetric decomposition," *IEEE Trans. Geosci. Remote Sens.*, vol. 51, no. 4, pp. 2201–2215, Apr. 2013.
[17] T. Jagdhuber, I. Hajnsek, and K. P. Papathanassiou, "An iterative generalized hybrid decomposition for soil moisture retrieval under vegetation cover using fully polarimetric SAR," *IEEE J. Sel. Topics Appl. Earth Observ. Remote Sens.*, vol. 8, no. 8, pp. 3911–3922, Aug. 2015.
[18] G. Di Martino, A. Iodice, A. Natale, and D. Riccio, "Polarimetric two-scale two-component model for the retrieval of soil moisture under moderate vegetation via L-band SAR data," *IEEE Trans. Geosci. Remote Sens.*, vol. 54, no. 4, pp. 2470–2491, Apr. 2016.
[19] X. Huang, J. Wang, and J. Shang, "An integrated surface parameter inversion scheme over agricultural fields at early growing stages by means of C-band polarimetric RADARSAT-2 imagery," *IEEE Trans. Geosci. Remote Sens.*, vol. 54, no. 5, pp. 2510–2528, May 2016.
[20] H. Wang, R. Magagi, and K. Goïta, "Potential of a two-component polarimetric decomposition at C-band for soil moisture retrieval over agricultural fields," *Remote Sens. Environ.*, vol. 217, no. Aug., pp. 38–51, 2018.
[21] C. Notarnicola, M. Angiulli, and F. Posa, "Use of radar and optical remotely sensed data for soil moisture retrieval over vegetated areas," *IEEE Trans. Geosci. Remote Sens.*, vol. 44, no. 4, pp. 925–935, Apr. 2006.
[22] E. Santi, S. Paloscia, S. Pettinato, and G. Fontanelli, "Application of artificial neural networks for the soil moisture retrieval from active and passive microwave spaceborne sensors," *Int. J. Appl. Earth Observ. Geoinf.*, vol. 48, pp. 61–73, 2016.
[23] F. Greifeneder *et al.*, "The added value of VH/VV polarization-ratio for global soil moisture estimations from scatterometer data," *IEEE J. Sel. Top. Appl. Earth Observ. Remote Sens.*, vol. 11, no. 10, pp. 3668–3679, Oct. 2018.
[24] S. Paloscia, S. Pettinato, E. Santi, C. Notarnicola, L. Pasolli, and A. Reppucci, "Soil moisture mapping using Sentinel-1 images: Algorithm and preliminary validation," *Remote Sens. Environ.*, vol. 134, pp. 234–248, 2013.
[25] R. Attarzadeh, J. Amini, C. Notarnicola, and F. Greifeneder, "Synergetic use of Sentinel-1 and Sentinel-2 data for soil moisture mapping at plot scale," *Remote Sens.*, vol. 10, no. 8, pp. 1–18, 2018.
[26] J. D. Ouellette *et al.*, "A time-series approach to estimating soil moisture from vegetated surfaces using L-band radar backscatter," *IEEE Trans. Geosci. Remote Sens.*, vol. 55, no. 6, pp. 3186–3193, Jun. 2017.
[27] A. Balenzano *et al.*, "On the use of temporal series of L-and X-band SAR data for soil moisture retrieval. Capitanata plain case study," *Eur. J. Remote Sens.*, vol. 46, no. 1, pp. 721–737, 2013.
[28] H. Shi *et al.*, "Soil moisture retrieval using a modified decomposition method and multi-incidence polarimetric SAR data," in *Proc. IGARSS IEEE Int. Geosci. Remote Sens. Symp.*, 2019, pp. 6957–6960.
[29] G. C. Topp, J. L. Davis, and A. P. Annan, "Electromagnetic determination of soil water content: Measurements in coaxial transmission lines," *Water Resour. Res.*, vol. 16, pp. 574–582, 1980.
[30] A. Freeman and S. L. Durden, "A three-component scattering model for polarimetric SAR data," *IEEE Trans. Geosci. Remote Sens.*, vol. 36, no. 3, pp. 963–973, May 1998.
[31] Y. Yamaguchi, T. Moriyama, M. Ishido, and H. Yamada, "Four-component scattering model for polarimetric SAR image decomposition," *IEEE Trans. Geosci. Remote Sens.*, vol. 43, no. 8, pp. 1699–1706, Aug. 2005.
[32] J. J. van Zyl, M. Arii, and Y. Kim, "Model-based decomposition of polarimetric SAR covariance matrices constrained for nonnegative eigenvalues," *IEEE Trans. Geosci. Remote Sens.*, vol. 49, no. 9, pp. 3452–3459, Sep. 2011.
[33] P. Dubois, J. van Zyl, and T. Engman, "Measuring soil moisture with imaging radars," *IEEE Trans. Geosci. Remote Sens.*, vol. 33, no. 4, pp. 915–926, Jul. 1995.
[34] Y. Oh, "Quantitative retrieval of soil moisture content and surface roughness from multipolarized radar observations of bare soil surfaces," *IEEE Trans. Geosci. Remote Sens.*, vol. 42, no. 3, pp. 596–601, Mar. 2004.
[35] S. Kim, H. Huang, L. Tsang, T. Jackson, H. McNairn, and J. van Zyl, "Soil moisture retrieval using L-band time-series SAR data from the SMAPVEX12 experiment," in *Proc. 10th Eur. Conf. Synthetic Aperture Radar*, 2014, pp. 1–4.
[36] H. Wang, R. Magagi, K. Goita, T. Jagdhuber, and I. Hajnsek, "Evaluation of simplified polarimetric decomposition for soil moisture retrieval over vegetated agricultural fields," *Remote Sens.*, vol. 8, no. 2, Feb. 2016, Art. no. 142.
[37] H. Wang, R. Magagi, K. Goita, and T. Jagdhuber, "Refining a polarimetric decomposition of multi-angular UAVSAR time series for soil moisture retrieval over low and high vegetated agricultural fields," *IEEE J. Sel. Topics Appl. Earth Observ. Remote Sens.*, vol. 12, no. 5, pp. 1431–1450, May 2019.
[38] D. Ratha, D. Mandal, V. Kumar, H. Mcnairn, A. Bhattacharya, and A. C. Frery, "A generalized volume scattering model-based vegetation index from polarimetric SAR data," *IEEE Geosci. Remote Sens. Lett.*, vol. 16, no. 11, pp. 1791–1795, Nov. 2019.
[39] D. Mandal *et al.*, "Assessment of rice growth conditions in a semi-arid region of India using the generalized radar vegetation index derived from RADARSAT-2 polarimetric SAR data," *Remote Sens. Environ.*, vol. 237, 2020, Art. no. 111561.

Hongtao Shi (Graduate Student Member, IEEE) received the B.S. degree in geographic information system and the M.S. degree in surveying and mapping from the China University of Petroleum (East China), Qingdao, China, in 2014 and 2017, respectively. He is currently working toward the Ph.D. degree in photogrammetry and remote sensing with the State Key Laboratory of Information Engineering, Wuhan University, Wuhan, China.

From October 2019 to November 2020, he was a Visiting Ph.D. Student with the University of Alicante (UA), Alicante, Spain. His research interests include surface and crop parameters estimation from polarimetric synthetic aperture radar (SAR) imagery.

Juan M. Lopez-Sanchez (Senior Member, IEEE) was born in Alicante, Spain, in 1972. He received the Ingeniero (M.S.) and Doctor Ingeniero (Ph.D.) degrees in telecommunication engineering from the Technical University of Valencia (UPV), Valencia, Spain, in 1996 and 2000, respectively.

From 1998 to 1999, he was as a Predoctoral Grantholder with the Space Applications Institute, Joint Research Centre of the European Commission, Ispra, Italy. Since 2000, he leads the Signals, Systems, and Telecommunication Group, University of Alicante, Alicante, Spain, where he is a Full Professor, since November 2011. He has coauthored more than 80 papers in refereed journals and more than 130 papers and presentations in international conferences and symposia. His main research interests include microwave remote sensing for inversion of biophysical parameters, polarimetric and interferometric techniques, SAR imaging algorithms, and applications of radar remote sensing in agriculture and geophysics.

Dr. Lopez-Sanchez was the recipient of the 2001 Indra Award for the best Ph.D. thesis about radar in Spain. From 2006 to 2012, he was the Chair of the Spanish Chapter of the IEEE Geoscience and Remote Sensing Society.

Jie Yang was born in Jingmen, China, in 1972. He received the B.S. degree in electronic and information engineering and M.S. degree in computer science from the Wuhan Technical University of Surveying and Mapping (WTUSM), Wuhan, China, in 1994 and 2000, respectively, and the Ph.D. degree in photogrammetry and remote sensing from Wuhan University, Wuhan, China, in 2004.

Since 2011, he has been a Research Fellow with the State Key Laboratory of Information Engineering in Surveying, Mapping, and Remote Sensing, Wuhan University. His research interests include polarimetric synthetic aperture radar image processing and interpretation and its applications in target detection, change detection, and disaster monitoring.

Pingxiang Li was born in Pingjiang, China, in 1964. He received the B.S. and M.S. degrees in photogrammetry and remote sensing from the Wuhan Technical University of Surveying and Mapping (WTUSM), Wuhan, China, in 1986 and 1994, respectively, and the Ph.D. degree in photogrammetry and remote sensing from Wuhan University, Wuhan, China, in 2003.

Since 2002, he has been a Research Fellow with the State Key Laboratory of Information Engineering in Surveying, Mapping, and Remote Sensing, Wuhan University. His research interests include synthetic aperture radar image processing,radiometric and polarimetric calibration, and its applications in disaster and agriculture monitoring.

Lingli Zhao (Member, IEEE) received the B.S. degree in geographic information systems from Zhengzhou University, Zhengzhou, China, in 2010, and the Ph.D. degree in photogrammetry and remote sensing from Wuhan University, Wuhan, China, in 2015.

She has been a Research Fellow with the School of Remote Sensing and Information Engineering, Wuhan University, since 2015. Her research interests include polarimetric SAR image processing and its applications in agriculture, wetland studies, disaster monitoring, and target detection.

Jinqi Zhao received the Ph.D. degree in photogrammetry and remote sensing from Wuhan University, Wuhan, China, in 2018.

He has been a Postdoctoral with the School of Resource and Environmental Sciences, Wuhan University, since 2018. His research interests include polarimetric SAR image processing and its applications in change detection, target extraction, and wetland monitoring.